Coherent Control of a Long-Lived Nuclear Memory Spin in a Germanium-Vacancy Multi-Qubit Node

Nick Grimm,[1,*] Katharina Senkalla,[1,*,†] Philipp J. Vetter,[1,*] Jurek Frey,[2,3] Prithvi Gundlapalli,[1] Tommaso Calarco,[4,5,6] Genko Genov,[1] Matthias M. Müller,[4] and Fedor Jelezko[1]

[1]*Institute for Quantum Optics, Ulm University, Albert-Einstein-Allee 11, 89081 Ulm, Germany*
[2]*Peter Grünberg Institute-Quantum Computing Analytics (PGI-12), Forschungszentrum Jülich GmbH, D-52425 Jülich, Germany*
[3]*Theoretical Physics, Saarland University, D-66123 Saarbrücken, Germany*
[4]*Peter Grünberg Institute-Quantum Control (PGI-8), Forschungszentrum Jülich GmbH, D-52425 Jülich, Germany*
[5]*Institute for Theoretical Physics, University of Cologne, D-50937 Cologne, Germany*
[6]*Dipartimento di Fisica e Astronomia, Università di Bologna, 40127 Bologna, Italy*

(Received 3 September 2024; accepted 9 December 2024; published 31 January 2025)

The ability to process and store information on surrounding nuclear spins is a major requirement for group-IV color center-based repeater nodes. We demonstrate coherent control of a ^{13}C nuclear spin strongly coupled to a negatively charged germanium-vacancy center in diamond with coherence times beyond 2.5 s at mK temperatures, which is the longest reported for group-IV defects. Detailed analysis allows us to model the system's dynamics, extract the coupling parameters, and characterize noise. We estimate an achievable memory time of 18.1 s with heating limitations considered, paving the way to successful applications as a quantum repeater node.

DOI: 10.1103/PhysRevLett.134.043603

Long-distance quantum communication paves the way to advanced quantum technologies including blind and distributed quantum computing for processing quantum information [1–4], quantum key distribution for secure communication [5–8], and quantum-enhanced metrology [9–12]. A key element to achieve this is the quantum repeater to mitigate losses in quantum channels [13].

Group-IV color centers in diamond have emerged as promising candidates for such repeater nodes [14] due to their efficient spin-photon interface [15–18]. This interface can be further enhanced by integration into nanophotonic devices and cavities [19–25]. To generate entanglement between distant nodes, these systems require long coherence times that are primarily limited by phonon-mediated dephasing in group-IV defects [26,27]. Innovations such as strain engineering [28–30] and the use of dilution refrigerators [31] have enabled coherence times of up to 20 ms [32–34]. Another key requirement is the ability to address nuclear spins, which can serve as long-lived quantum memory and thus extend the entanglement distance. This has been effectively demonstrated with the silicon-vacancy center (SiV), which achieved entanglement across a metropolitan fiber network by utilizing the inherent ^{29}Si nuclear spin [35].

On the other hand surrounding ^{13}C nuclear spins can also act as memory qubits across all group-IV platforms and additionally can be used to form a register. Such quantum register would allow for quantum error correction (QEC) [36,37] and entanglement purification protocols [13,38], which are important for quantum networking. With a natural abundance of 1.1%, ^{13}C nuclei are an easily accessible resource providing a range of possible coupling strengths [39]. While initialization and coherent control of ^{13}C spins was already demonstrated for the SiV [30,40–42], this is an ongoing challenge for heavier group-IV defects [43], that can operate at elevated temperatures without loss of coherence [18,44–46].

In this work, we focus on a multi-qubit node comprising a negatively charged germanium-vacancy (GeV) and a strongly coupled ^{13}C nucleus. We characterize the hyperfine interaction through optically detected magnetic resonance (ODMR) measurements and a detailed numerical model. Because of the strong hyperfine interaction, we can initialize the nuclear spin up to 95% utilizing a power-efficient microwave spin pumping scheme. Additionally, narrow-band microwave (mw) and radio frequency (rf) pulses enable conditional flipping of the electron and nuclear spin. This allows us to efficiently swap the electron and nuclear eigenstates, leading to a projection-SWAP gate, that can be used for initialization and readout. We demonstrate coherent control of the ^{13}C spin using direct rf manipulation, achieving nuclear Rabi frequencies up to 11.73 kHz. Through application of dynamical decoupling (DD) sequences, we can prolong the nuclear spin's dephasing time of $T_2^* = 2$ ms by more than three orders of magnitude to $T_2 = 2.57$ s, marking the longest achieved

*These authors contributed equally to this work.
†Contact author: katharina.senkalla@uni-ulm.de

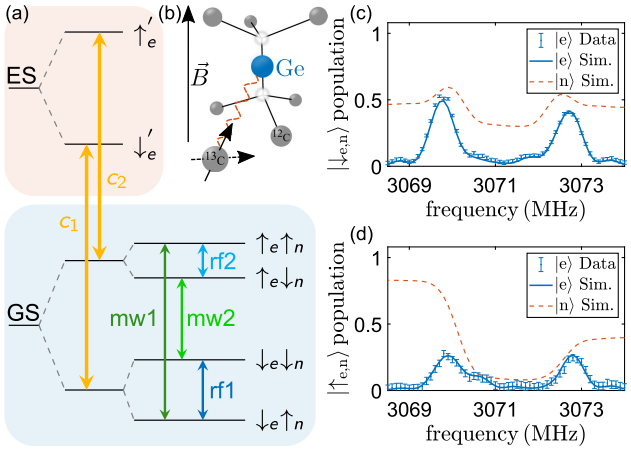

FIG. 1. Description of the system. (a) Reduced energy level scheme of the GeV showing the lower orbital branch in the ground state (GS) and excited state (ES). Strong hyperfine coupling to a ^{13}C nuclear spin leads to an additional splitting. (b) Schematic of GeV aligned with external magnetic field, showing electron spin-state-dependent nuclear spin quantization axes. Pulsed ODMR measurements with descending frequency sweep direction where the electron is reinitialized into $|\uparrow_e\rangle$ via optical transition c_1 (c) and into $|\downarrow_e\rangle$ via c_2 (d). The red dashed line corresponds to the simulated nuclear spin evolution.

coherence time of a controllable nuclear memory spin for all group-IV defects [35]. We further provide a realistic estimation of the longest achievable memory time of $T_2^{\mathrm{mem}} = 18.1$ s considering noise errors modeled by Ornstein-Uhlenbeck (OU) processes [33,47], the T_1 time of the GeV electron spin, and experimental heating limitations.

The system—We perform the experiments on a high pressure high temperature (HPHT) grown diamond with natural abundance of ^{13}C. Our multi-qubit node features a naturally incorporated GeV strongly coupled to a ^{13}C nuclear spin, operated in a dilution refrigerator [33,48]. In a magnetic field aligned to the defect's axis, this forms a four-level system with selective transitions as depicted in Fig. 1(a). The electron (nuclear) spin can be coherently controlled via mw (rf) driving fields, supplied through a 20 μm thick copper wire spanned over the diamond. Resonant addressing at the optical transitions $c_{1,2}$ allows for high fidelity initialization and readout of the electron spin. Further details of the experimental implementation can be found in Ref. [48].

The evolution of the system can be characterized in the rotating frame of the GeV center's electron spin by the Hamiltonian

$$H = \Delta S_z + \Omega_e S_x - \gamma_n B_z I_z + A_{zx} S_z I_x + A_{zz} S_z I_z, \quad (1)$$

under the secular approximation [64], excluding the nuclear rf driving fields for readability. The parameters A_{zx} and A_{zz} correspond to the hyperfine coupling parameters, $S_j(I_j)$ with $j \in \{x, y, z\}$ are the spin operators on the GeV electron spin (^{13}C nuclear spin), γ_n is the gyromagnetic ratio of the nuclear spin, Ω_e is the Rabi frequency on the electron spin transition, and Δ is the detuning of the mw driving field frequency from the transition frequency of the bare GeV electron spin, i.e., in the absence of ^{13}C couplings (in angular frequency units) [48].

The strong hyperfine interaction leads to an additional splitting of the electron spin states that can be observed in a pulsed ODMR measurement. Figure 1(c) shows the spectrum for $|\uparrow_e\rangle$ and Fig. 1(d) for $|\downarrow_e\rangle$, with $\Omega_e = (2\pi)349$ kHz for the descending frequency sweep direction. The data corresponds to the averaged fluorescence signal of ~3470 repetitions where we perform a consecutive Rabi measurement after each repetition for normalization [48]. We observe a significant difference in shape and amplitude of the spectra, that is heavily influenced by the frequency sweep direction [48].

To identify the underlying dynamics we perform a total of four ODMR measurements, two for each electron spin state, differing by their frequency sweep direction, and fit them with a numerical model. The model describes the full interaction between the electron and nuclear spin, including dephasing and the optical reset of the electron spin. Full details can be found in Supplemental Material [48]. The fit result is shown in Fig. 1(c) for $|\uparrow_e\rangle$ and in Fig. 1(d) for $|\downarrow_e\rangle$ by the blue lines, achieving a R^2 of 0.9854 and 0.9568, respectively. From the fit result we determine the magnetic field to be $B_z = (97.159 \pm 0.005)$ mT which slightly deviates from the set 100 mT due to the diamond placement in the vector magnet. Using the nuclear transition frequencies $\omega_{\mathrm{rf2}} = (2\pi)(493.62 \pm 0.04)$ kHz and $\omega_{\mathrm{rf1}} = (2\pi)(2489.73 \pm 0.06)$ kHz from a nuclear Ramsey experiment (detailed below) we can estimate the hyperfine coupling parameters according to

$$A_{zz} = \frac{\omega_{\mathrm{rf1}}^2 - \omega_{\mathrm{rf2}}^2}{2\gamma_n B_z} \quad (2)$$

and

$$A_{zx} = \sqrt{4\omega_{\mathrm{rf2}}^2 - (A_{zz} - 2\gamma_n B_z)^2}. \quad (3)$$

This leads to $A_{zx} = 2\pi(602.81 \pm 0.27)$ kHz and $A_{zz} = 2\pi(2862.34 \pm 0.14)$ kHz.

Depending on the electron spin state, the strong hyperfine interaction changes the nuclear spin's quantization axis significantly, as illustrated in Fig. 1(b). Rotation of the electron spin, e.g., in the form of a narrow-band (detuned) π pulse, can thus alter the nuclear spin state, which in turn affects the electron spin population transfer. During a free evolution time, i.e., during the 5.5 ms long reinitialization of the electron spin, the nuclear spin oscillates around the corresponding quantization axis and dephases. Its simulated evolution over the course of the ODMR measurement is shown by the dashed red line, revealing a significant

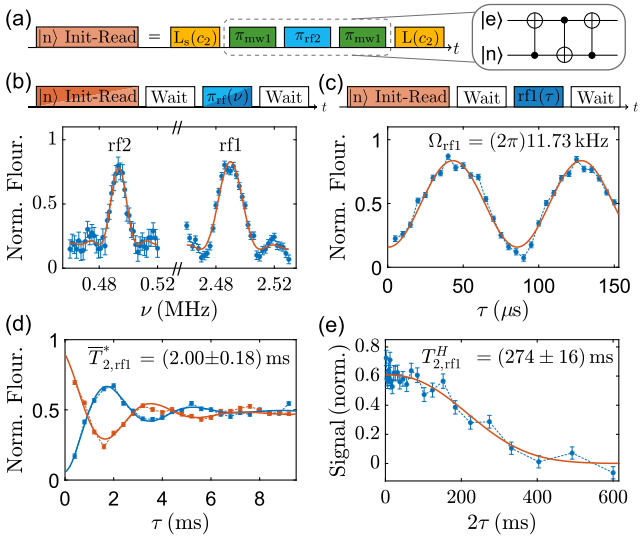

FIG. 2. Coherent control of the ^{13}C nuclear spin. (a) Pulse sequence for nuclear spin initialization and readout in the $|\downarrow_e\rangle$ manifold, where L_s indicates an initializing laser element without recording the corresponding photons [48]. (b) Pulse sequence and measurements for detecting nuclear transition frequencies, with added waiting periods to limit heat load. Nuclear spin initialization and readout in the $|\uparrow_e\rangle$ manifold (dark orange) uses laser frequency c_1 and microwave elements mw2 instead. The following nuclear spin measurements are conducted in the $|\downarrow_e\rangle$ manifold: (c) Demonstration of coherent control by the ^{13}C Rabi experiment. (d) Nuclear Ramsey measurement, with the red line showing a Ramsey measurement using a 180° phase-shifted final $\pi/2$ rf pulse. (e) Differential signal of a nuclear Hahn echo with corresponding fit (red line).

polarization buildup in the $|\downarrow_e\rangle$ manifold [Fig. 1(d)] due to spin pumping.

The spin pumping is facilitated by the strong hyperfine interaction that leads to the large splitting ω_{rf1} of the nuclear spin states for $|\downarrow_e\rangle$. This splitting allows the microwave pulse to selectively address one of the hyperfine levels while leaving the other untouched. The strong A_{zx} coupling then enables the simultaneous flipping of both spins, allowing for the otherwise forbidden transitions [53]. As the laser resets the electron spin, the repetitive application of a microwave and laser pulse leads to polarization of the nuclear spin. At sub-Kelvin temperatures, the nuclear spin's polarization survives the entire sequence and thus the frequency sweep direction alters the observed shape. For $|\uparrow_e\rangle$ shown in Fig. 1(c), the polarization buildup is significantly less efficient as the small splitting ω_{rf2} prevents the selective addressing of the hyperfine levels with the chosen Rabi frequency.

We can exploit the spin pumping process to experimentally initialize the nuclear spin for $|\downarrow_e\rangle$ with a state preparation fidelity of 95% by repeatedly applying a resonant mw pulse at ω_{mw2} and a subsequent laser pulse 15 times, closely matching our simulation results [48]. While this method is less time-efficient compared to the projection-SWAP gate shown in the following section, it achieves nuclear spin polarization without the need of resonant rf pulses. Thus, it offers an easily accessible way of initializing the system to its eigenstates while reducing the heat load. Additionally, the application of optimal control [65–67] in our numerical simulation suggests that a fidelity of up to 99% could be achieved, using a single optimized pulse [48].

Coherent control of the nuclear memory spin—To establish coherent control over our nuclear spin, we construct a projection-SWAP gate based on three CNOT gates, as sketched in Fig. 2(a). The large A_{zz} hyperfine coupling allows us to implement these CNOT gates up to a phase through narrow-band π-pulse gates that flip the electron spin conditional on the nuclear spin and vice versa. The limited electron dephasing time of $T^*_{2,e} = 1.43\ \mu\mathrm{s}$ [33] poses challenges for a direct transfer of coherent states, given the dozens of microseconds long $C_e\mathrm{NOT}_n$ gate. Nonetheless, we can use the projection-SWAP gate to efficiently initialize the nuclear spin to its eigenstates and read out the projection of any arbitrary nuclear spin state onto $|\uparrow_n\rangle$ or $|\downarrow_n\rangle$.

The projection-SWAP gate requires knowledge of the nuclear transition frequency and π rf pulse length of the $C_e\mathrm{NOT}_n$ gate. To determine these parameters the rf pulse can be sandwiched in between the previously introduced nuclear spin pumping scheme for initialization and a $C_n\mathrm{NOT}_e$ combined with a subsequent laser pulse for readout. Alternatively, the required parameters can be obtained by iteratively maximizing the contrast of the rf-frequency (ν) sweep experiment in Fig. 2(b) and the rf-Rabi experiment in Fig. 2(c). We obtain a nuclear Rabi frequency of (11.73 ± 0.14) kHz for ω_{rf1}, which we can use to construct any arbitrary single qubit nuclear spin gate, establishing full coherent control over the nuclear subspace.

To characterize the quality of our nuclear memory storage, we start by measuring the nuclear dephasing time in a Ramsey experiment, consisting of two $\pi/2$ rf pulses with a variable interpulse duration. Figure 2(d) illustrates that measurements are performed in an alternating manner, using a final $\pi/2$ rf pulse with 0° (x) or 180° ($-x$) phase to project onto the different eigenstates. As this helps to minimize effects like laser fluctuations, all of the following measurements are performed in this fashion, while only the normalized differential signal is shown. The oscillations of the signal shown in Fig. 2(d) arise from controlled detuning of the applied field from the nuclear transitions, which allows us to infer their frequencies with high accuracy to $\omega_{\mathrm{rf1}} = (2\pi)(2489.73 \pm 0.06)$ kHz and $\omega_{\mathrm{rf2}} = (2\pi)(493.62 \pm 0.04)$ kHz [48].

Through application of a Hahn echo sequence [68] we can decouple the nuclear spin from slowly varying magnetic fields, resulting in a coherence time

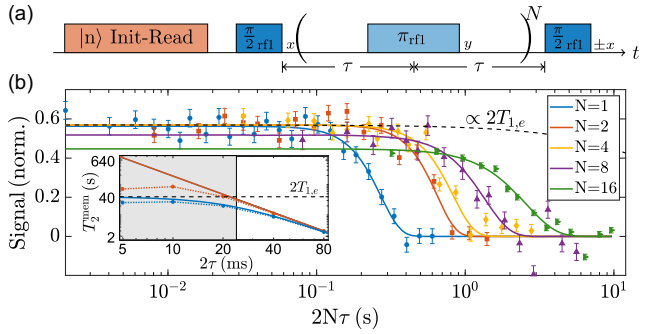

FIG. 3. Coherence time measurements on ^{13}C. (a) Pulse sequence of the nuclear CPMG sequence with the number of refocusing pulses N and interpulse spacing τ in alternating manner (indicated by $\pm x$ on final $\pi/2$ rf pule). (b) Corresponding coherence time measurements for fixed N with their respective fit. The black dashed line represents the theoretical limit of the electron relaxation time $T_{1,e}$. Inset: Simulation of the limit of the expected memory time when using different pulse separation times 2τ, assuming an OU noise process. The blue (red) line shows the expected memory time with (without) taking into account $T_{1,e}$ relaxation. The white area emphasizes feasible pulse spacings that avoid excessive heating in our current setup. The dotted curves show numerical simulations of the memory time with the XY8 sequence that take pulse errors into account [48].

of $T_2^H = (274 \pm 16)$ ms, as displayed in Fig. 2(e)—an improvement of more than 2 orders of magnitude compared to $T^*_{2,\mathrm{rf1}} = (2.00 \pm 0.18)$ ms obtained by the Ramsey measurement.

Analysis of the nuclear spin quantum memory—The ^{13}C nuclear spin coherence time can be further extended by dynamical decoupling protocols [69–74]. We apply the CPMG sequence [70] for our experiments, similar to previous work [33], as it can also be used to characterize the environmental noise. For this purpose, we start by measuring the coherence time for different orders N (equal to the number of refocusing pulses), while sweeping the pulse spacing τ. The corresponding sequence is shown in Fig. 3(a). We achieve a coherence time up to $T_2 = (2.57 \pm 0.19)$ s for $N = 16$, shown in green in Fig. 3(b), which marks the so far longest measured nuclear spin coherence time for any group-IV defect.

The overall contrast decays with increasing N, which can be explained by the insufficient long-term stability of the laser hardware over the extended measurement period (> 1 d for $N = 16$) or by minor pulse imperfections. To investigate the impact of pulse errors, we perform an additional measurement using the XY8 sequence, known for its robustness [71]. The resulting coherence time of $T_2^{\mathrm{XY8}} = (1.49 \pm 0.10)$ s [48] is consistent with the CPMG-8 sequence, $T_2^{\mathrm{CPMG8}} = (1.36 \pm 0.14)$ s, suggesting that pulse errors are not yet limiting our coherence time.

Building on these results, we assess the memory capabilities of our system. We model the effects of environmental and amplitude noise using an Ornstein-Uhlenbeck process, as outlined in previous work [33] and further elaborated in Ref. [48]. The inset of Fig. 3(b) shows the possible ^{13}C memory time, using a conservative estimate of the noise correlation time [48], and accounting for pulse errors and heating limitations in our setup. The main limiting factors for the memory time are heating and $T_{1,e}$ relaxation. We estimate that a pulse spacing of $2\tau = 24$ ms and higher causes negligible heating and is feasible for dynamical decoupling. This allows for a memory time of $T_2^{\mathrm{mem}} = 18.1$ s [48]. Reducing pulse separation to around 10 ms by improving the effective cooling of the sample would boost the memory time to $T_2^{\mathrm{mem}} \approx 28$ s where pulse errors with the XY8 sequence start to play a role due to the large number of pulses. Application of higher order sequences like KDD or the UR family [75–77] can in principle boost the memory time limit even closer to the $T_{1,e}$ limit of 41.4 s.

Discussion—The proximity of a ^{13}C nuclear spin to the GeV center within our multi-qubit node results in a strong A_{zx} and A_{zz} hyperfine coupling between the nuclear and electron spin. While this influences fundamental pulsed experiments, we show how to leverage it to determine the system's Hamiltonian with its hyperfine parameters by providing an elaborate numerical model which can be fitted to a pulsed ODMR measurement.

We use the insights of the model to implement a cooling power-efficient spin pumping scheme to initialize the ^{13}C nuclear spin with the so far highest fidelity of 95% utilizing a group-IV defect. This approach is particularly advantageous as it does not require precise prior knowledge of the coupling parameters and addresses the constraints of cooling power in dilution refrigerators. Although this protocol takes longer compared to the demonstrated projection-SWAP gate, quantum optimal control [65–67,78] offers a potential path to even shorter gate times and higher fidelities [48]. Our spin pumping scheme and numerical model can be seamlessly applied to any group-IV color center with $S = 1/2$, provided it strongly interacts with a nonaxial nuclear $I = 1/2$ spin.

Direct driving of the ^{13}C nuclear spin with resonant rf pulses allows precise one-qubit operations, bypassing the limitations of using the electron spin as an intermediary [41,42], and facilitates straightforward implementation of a $\mathrm{C}_e\mathrm{NOT}_n$. The strong A_{zz} coupling enables the implementation of a $\mathrm{C}_n\mathrm{NOT}_e$ in a similar fashion through a narrow-band microwave pulse. Combining both of these gates allows us to easily implement a projection-SWAP that can be used to initialize the nuclear spin and readout the projection of its state along its quantization axis. In its current form, our projection-SWAP gate cannot swap coherent states as the $\mathrm{C}_e\mathrm{NOT}_n$ length significantly exceeds the electron's dephasing time. While protocols that account for the low dephasing time by interleaving the gate with refocusing pulses [30,79] are hindered by our strong A_{zx} interaction, advanced protocols [80–82] or quantum optimal

control might also provide a solution to overcome this problem [83,84].

Conclusion and outlook—We demonstrate coherent control over the nuclear spin of ^{13}C, strongly coupled to a GeV center electron spin. We perform dynamical decoupling to protect the nuclear spin from environmental noise for more than 2.5 s, marking the so far longest achieved nuclear memory time for all group-IV defect systems. This is achieved with a 60 times lower number of refocusing pulses than previously required for coherence times beyond 2 s for group-IV defects [30]. The low duty cycle results in overall reduced heat load, which is critical for operation in dilution refrigerators. To estimate the memory performance, we include these heating effects, electron spin $T_{1,e}$ relaxation, pulse errors, and environmental noise simulated by Ornstein-Uhlenbeck processes in a numerical model. We can thus provide a realistic upper limit of 18.1 s as an achievable memory time with our current setup, which can realistically be extended to several tens of seconds through modifications, such as optimizing thermal grounding, improving the mw and rf delivery, or using superconducting structures [34].

Such a long living quantum memory facilitates the generation of multidimensional cluster states [85], which are important in the realm of measurement based quantum computing or long distance quantum communication. Furthermore, integrating our multi-qubit node into a nanophotonic cavity could facilitate the implementation of recently demonstrated direct photon-nuclear entanglement gates [30], which have achieved successful entanglement generation over distances of 35 km [35]. Finally, leveraging weakly coupled ^{13}C spins, which can be actively decoupled from the electron spin, would allow for scaling up the register [36,43,86–89] and pave the way for performing QEC [36,37] and entanglement purification protocols [13,38].

Acknowledgments—We thank Frank Wilhelm-Mauch, Rémi Blinder, Lev Kazak, and Petr Siyushev for helpful discussions and technical support. Further, we thank Yuri N. Palyanov, Igor N. Kupriyanov, and Yuri M. Borzdov for providing the sample used in this work. The authors acknowledge support by the state of Baden-Württemberg through bwHPC. This work was funded by the German Federal Ministry of Research (BMBF) by future cluster QSENS (No. 03ZK110AB) and projects DE-Brill (No. 13N16207), SPINNING (No. 13N16210 and No. 13N16215), DIAQNOS (No. 13N16463), Quamapolis (No. 13N15375), and EXTRASENS (No. 731473 and 101017733) DLR via project QUASIMODO (No. 50WM2170), Deutsche Forschungsgemeinschaft (DFG) via Projects No. 386028944, No. 445243414, No. 491245864, and No. 387073854. This project has also received funding from the European Union's HORIZON Europe program via projects QuMicro (No. 101046911), SPINUS (No. 101135699), C-QuENS (No. 101135359), QCIRCLE (No. 101059999) and FLORIN (No. 101086142), European Research Council (ERC) via Synergy grant HyperQ (No. 856432), Competence Center Quantum Computing Baden-Württemberg, and Carl-Zeiss-Stiftung via the Center of Integrated Quantum Science and technology (IQST) and project Utrasens-Vir (No. P2022-06-007) and QPhoton, as well as the Helmholtz Validation Fund project "Qruise" (HVF-00096).

[1] N. H. Nickerson, J. F. Fitzsimons, and S. C. Benjamin, Freely scalable quantum technologies using cells of 5-to-50 qubits with very lossy and noisy photonic links, Phys. Rev. X **4**, 041041 (2014).
[2] H. Choi, M. Pant, S. Guha, and D. Englund, Percolation-based architecture for cluster state creation using photon-mediated entanglement between atomic memories, npj Quantum Inf. **5**, 104 (2019).
[3] D. Cuomo, M. Caleffi, and A. S. Cacciapuoti, Towards a distributed quantum computing ecosystem, IET Quantum Commun. **1**, 3 (2020).
[4] P. Drmota, D. P. Nadlinger, D. Main, B. C. Nichol, E. M. Ainley, D. Leichtle, A. Mantri, E. Kashefi, R. Srinivas, G. Araneda, C. J. Ballance, and D. M. Lucas, Verifiable blind quantum computing with trapped ions and single photons, Phys. Rev. Lett. **132**, 150604 (2024).
[5] A. K. Ekert, Quantum cryptography based on Bell's theorem, Phys. Rev. Lett. **67**, 661 (1991).
[6] C. Elliott, Building the quantum network, New J. Phys. **4**, 46 (2002).
[7] H.-K. Lo, M. Curty, and K. Tamaki, Secure quantum key distribution, Nat. Photonics **8**, 595 (2014).
[8] F. Xu, X. Ma, Q. Zhang, H.-K. Lo, and J.-W. Pan, Secure quantum key distribution with realistic devices, Rev. Mod. Phys. **92**, 025002 (2020).
[9] D. Gottesman, T. Jennewein, and S. Croke, Longer-baseline telescopes using quantum repeaters, Phys. Rev. Lett. **109**, 070503 (2012).
[10] P. Komar, E. M. Kessler, M. Bishof, L. Jiang, A. S. Sørensen, J. Ye, and M. D. Lukin, A quantum network of clocks, Nat. Phys. **10**, 582 (2014).
[11] E. T. Khabiboulline, J. Borregaard, K. De Greve, and M. D. Lukin, Optical interferometry with quantum networks, Phys. Rev. Lett. **123**, 070504 (2019).
[12] Y. Yang, B. Yadin, and Z.-P. Xu, Quantum-enhanced metrology with network states, Phys. Rev. Lett. **132**, 210801 (2024).
[13] H.-J. Briegel, W. Dür, J. I. Cirac, and P. Zoller, Quantum repeaters: The role of imperfect local operations in quantum communication, Phys. Rev. Lett. **81**, 5932 (1998).
[14] M. Ruf, N. H. Wan, H. Choi, D. Englund, and R. Hanson, Quantum networks based on color centers in diamond, J. Appl. Phys. **130**, 070901 (2021).
[15] L. J. Rogers, K. D. Jahnke, M. H. Metsch, A. Sipahigil, J. M. Binder, T. Teraji, H. Sumiya, J. Isoya, M. D. Lukin, P. Hemmer, and F. Jelezko, All-optical initialization, readout, and coherent preparation of single silicon-vacancy spins in diamond, Phys. Rev. Lett. **113**, 263602 (2014).

[16] P. Siyushev, M. H. Metsch, A. Ijaz, J. M. Binder, M. K. Bhaskar, D. D. Sukachev, A. Sipahigil, R. E. Evans, C. T. Nguyen, M. D. Lukin, P. R. Hemmer, Y. N. Palyanov, I. N. Kupriyanov, Y. M. Borzdov, L. J. Rogers, and F. Jelezko, Optical and microwave control of germanium-vacancy center spins in diamond, Phys. Rev. B **96**, 081201(R) (2017).

[17] J. Görlitz, D. Herrmann, G. Thiering, P. Fuchs, M. Gandil, T. Iwasaki, T. Taniguchi, M. Kieschnick, J. Meijer, M. Hatano *et al.*, Spectroscopic investigations of negatively charged tin-vacancy centres in diamond, New J. Phys. **22**, 013048 (2020).

[18] P. Wang, L. Kazak, K. Senkalla, P. Siyushev, R. Abe, T. Taniguchi, S. Onoda, H. Kato, T. Makino, M. Hatano, F. Jelezko, and T. Iwasaki, Transform-limited photon emission from a lead-vacancy center in diamond above 10 K, Phys. Rev. Lett. **132**, 073601 (2024).

[19] C. Bradac, W. Gao, J. Forneris, M. E. Trusheim, and I. Aharonovich, Quantum nanophotonics with group IV defects in diamond, Nat. Commun. **10**, 5625 (2019).

[20] A. Sipahigil, R. E. Evans, D. D. Sukachev, M. J. Burek, J. Borregaard, M. K. Bhaskar, C. T. Nguyen, J. L. Pacheco, H. A. Atikian, C. Meuwly *et al.*, An integrated diamond nanophotonics platform for quantum-optical networks, Science **354**, 847 (2016).

[21] M. K. Bhaskar, D. D. Sukachev, A. Sipahigil, R. E. Evans, M. J. Burek, C. T. Nguyen, L. J. Rogers, P. Siyushev, M. H. Metsch, H. Park, F. Jelezko, M. Lončar, and M. D. Lukin, Quantum nonlinear optics with a germanium-vacancy color center in a nanoscale diamond waveguide, Phys. Rev. Lett. **118**, 223603 (2017).

[22] A. E. Rugar, S. Aghaeimeibodi, D. Riedel, C. Dory, H. Lu, P. J. McQuade, Z.-X. Shen, N. A. Melosh, and J. Vučković, Quantum photonic interface for tin-vacancy centers in diamond, Phys. Rev. X **11**, 031021 (2021).

[23] L. Antoniuk, N. Lettner, A. P. Ovvyan, S. Haugg, M. Klotz, H. Gehring, D. Wendland, V. N. Agafonov, W. H. Pernice, and A. Kubanek, All-optical spin access via a cavity-broadened optical transition in on-chip hybrid quantum photonics, Phys. Rev. Appl. **21**, 054032 (2024).

[24] R. A. Parker, J. Arjona Martínez, K. C. Chen, A. M. Stramma, I. B. Harris, C. P. Michaels, M. E. Trusheim, M. Hayhurst Appel, C. M. Purser, W. G. Roth *et al.*, A diamond nanophotonic interface with an optically accessible deterministic electronuclear spin register, Nat. Photonics **18**, 156 (2024).

[25] R. Zifkin, C. D. Rodríguez Rosenblueth, E. Janitz, Y. Fontana, and L. Childress, Lifetime reduction of single germanium-vacancy centers in diamond via a tunable open microcavity, PRX Quantum **5**, 030308 (2024).

[26] B. Pingault, D.-D. Jarausch, C. Hepp, L. Klintberg, J. N. Becker, M. Markham, C. Becher, and M. Atatüre, Coherent control of the silicon-vacancy spin in diamond, Nat. Commun. **8**, 15579 (2017).

[27] I. B. W. Harris and D. Englund, Coherence of group-IV color centers, Phys. Rev. B **109**, 085414 (2024).

[28] S. Meesala, Y.-I. Sohn, B. Pingault, L. Shao, H. A. Atikian, J. Holzgrafe, M. Gündoğan, C. Stavrakas, A. Sipahigil, C. Chia, R. Evans, M. J. Burek, M. Zhang, L. Wu, J. L. Pacheco, J. Abraham, E. Bielejec, M. D. Lukin, M. Atatüre, and M. Lončar, Strain engineering of the silicon-vacancy center in diamond, Phys. Rev. B **97**, 205444 (2018).

[29] Y.-I. Sohn, S. Meesala, B. Pingault, H. A. Atikian, J. Holzgrafe, M. Gündoğan, C. Stavrakas, M. J. Stanley, A. Sipahigil, J. Choi *et al.*, Controlling the coherence of a diamond spin qubit through its strain environment, Nat. Commun. **9**, 2012 (2018).

[30] P.-J. Stas, Y. Q. Huan, B. Machielse, E. N. Knall, A. Suleymanzade, B. Pingault, M. Sutula, S. W. Ding, C. M. Knaut, D. R. Assumpcao *et al.*, Robust multi-qubit quantum network node with integrated error detection, Science **378**, 557 (2022).

[31] H. Zu, W. Dai, and A. De Waele, Development of dilution refrigerators—a review, Cryogenics **121**, 103390 (2022).

[32] D. D. Sukachev, A. Sipahigil, C. T. Nguyen, M. K. Bhaskar, R. E. Evans, F. Jelezko, and M. D. Lukin, Silicon-vacancy spin qubit in diamond: A quantum memory exceeding 10 ms with single-shot state readout, Phys. Rev. Lett. **119**, 223602 (2017).

[33] K. Senkalla, G. Genov, M. H. Metsch, P. Siyushev, and F. Jelezko, Germanium vacancy in diamond quantum memory exceeding 20 ms, Phys. Rev. Lett. **132**, 026901 (2024).

[34] I. Karapatzakis, J. Resch, M. Schrodin, P. Fuchs, M. Kieschnick, J. Heupel, L. Kussi, C. Sürgers, C. Popov, J. Meijer, C. Becher, W. Wernsdorfer, and D. Hunger, Microwave control of the tin-vacancy spin qubit in diamond with a superconducting waveguide, Phys. Rev. X **14**, 031036 (2024).

[35] C. Knaut, A. Suleymanzade, Y.-C. Wei, D. Assumpcao, P.-J. Stas, Y. Huan, B. Machielse, E. Knall, M. Sutula, G. Baranes *et al.*, Entanglement of nanophotonic quantum memory nodes in a telecom network, Nature (London) **629**, 573 (2024).

[36] T. H. Taminiau, J. Cramer, T. van der Sar, V. V. Dobrovitski, and R. Hanson, Universal control and error correction in multi-qubit spin registers in diamond, Nat. Nanotechnol. **9**, 171 (2014).

[37] T. Unden, P. Balasubramanian, D. Louzon, Y. Vinkler, M. B. Plenio, M. Markham, D. Twitchen, A. Stacey, I. Lovchinsky, A. O. Sushkov, M. D. Lukin, A. Retzker, B. Naydenov, L. P. McGuinness, and F. Jelezko, Quantum metrology enhanced by repetitive quantum error correction, Phys. Rev. Lett. **116**, 230502 (2016).

[38] N. Kalb, A. A. Reiserer, P. C. Humphreys, J. J. Bakermans, S. J. Kamerling, N. H. Nickerson, S. C. Benjamin, D. J. Twitchen, M. Markham, and R. Hanson, Entanglement distillation between solid-state quantum network nodes, Science **356**, 928 (2017).

[39] A. P. Nizovtsev, S. Y. Kilin, A. L. Pushkarchuk, V. A. Pushkarchuk, S. A. Kuten, O. A. Zhikol, S. Schmitt, T. Unden, and F. Jelezko, Non-flipping ^{13}C spins near an NV center in diamond: Hyperfine and spatial characteristics by density functional theory simulation of the C510 [NV] H252 cluster, New J. Phys. **20**, 023022 (2018).

[40] M. H. Metsch, K. Senkalla, B. Tratzmiller, J. Scheuer, M. Kern, J. Achard, A. Tallaire, M. B. Plenio, P. Siyushev, and F. Jelezko, Initialization and readout of nuclear spins via a negatively charged silicon-vacancy center in diamond, Phys. Rev. Lett. **122**, 190503 (2019).

[41] C. T. Nguyen, D. D. Sukachev, M. K. Bhaskar, B. Machielse, D. S. Levonian, E. N. Knall, P. Stroganov, R. Riedinger, H. Park, M. Lončar, and M. D. Lukin, Quantum network nodes based on diamond qubits with an efficient nanophotonic interface, Phys. Rev. Lett. **123**, 183602 (2019).
[42] S. Maity, B. Pingault, G. Joe, M. Chalupnik, D. Assumpção, E. Cornell, L. Shao, and M. Lončar, Mechanical control of a single nuclear spin, Phys. Rev. X **12**, 011056 (2022).
[43] H. K. Beukers, C. Waas, M. Pasini, H. B. van Ommen, N. Codreanu, J. M. Brevoord, T. Turan, M. Iuliano, Z. Ademi, T. H. Taminiau *et al.*, Control of solid-state nuclear spin qubits using an electron spin-1/2, arXiv:2409.08977.
[44] R. Debroux, C. P. Michaels, C. M. Purser, N. Wan, M. E. Trusheim, J. Arjona Martínez, R. A. Parker, A. M. Stramma, K. C. Chen, L. de Santis, E. M. Alexeev, A. C. Ferrari, D. Englund, D. A. Gangloff, and M. Atatüre, Quantum control of the tin-vacancy spin qubit in diamond, Phys. Rev. X **11**, 041041 (2021).
[45] E. I. Rosenthal, C. P. Anderson, H. C. Kleidermacher, A. J. Stein, H. Lee, J. Grzesik, G. Scuri, A. E. Rugar, D. Riedel, S. Aghaeimeibodi, G. H. Ahn, K. Van Gasse, and J. Vučković, Microwave spin control of a tin-vacancy qubit in diamond, Phys. Rev. X **13**, 031022 (2023).
[46] X. Guo, A. M. Stramma, Z. Li, W. G. Roth, B. Huang, Y. Jin, R. A. Parker, J. Arjona Martínez, N. Shofer, C. P. Michaels, C. P. Purser, M. H. Appel, E. M. Alexeev, T. Liu, A. C. Ferrari, D. D. Awschalom, N. Delegan, B. Pingault, G. Galli, F. J. Heremans, M. Atatüre, and A. A. High, Microwave-based quantum control and coherence protection of tin-vacancy spin qubits in a strain-tuned diamond-membrane heterostructure, Phys. Rev. X **13**, 041037 (2023).
[47] G. E. Uhlenbeck and L. S. Ornstein, On the theory of the Brownian motion, Phys. Rev. **36**, 823 (1930).
[48] See Supplemental Material at http://link.aps.org/supplemental/10.1103/PhysRevLett.134.043603 for details on the sample and setup, for the numerical simulation for hyperfine parameter extraction, nuclear spin pumping, optimal control simulations, further details on nuclear spin coherence experiments, noise calibration and numerical simulations on nuclear spin memory time with Refs. [49–63] included therein.
[49] Y. N. Palyanov, I. N. Kupriyanov, Y. M. Borzdov, and N. V. Surovtsev, Germanium: A new catalyst for diamond synthesis and a new optically active impurity in diamond, Sci. Rep. **5**, 14789 (2015).
[50] M. A. Nielsen and I. L. Chuang, *Quantum Computation and Quantum Information* (Cambridge University Press, Cambridge, England, 2010).
[51] G. Thiering and A. Gali, *Ab initio* magneto-optical spectrum of group-IV vacancy color centers in diamond, Phys. Rev. X **8**, 021063 (2018).
[52] R. Storn and K. Price, Differential evolution–a simple and efficient heuristic for global optimization over continuous spaces, J. Global Optim. **11**, 341 (1997).
[53] A. Schweiger and G. Jeschke, *Principles of Pulse Electron Paramagnetic Resonance* (Oxford University Press, New York, 2001).
[54] J. F. Barry, J. M. Schloss, E. Bauch, M. J. Turner, C. A. Hart, L. M. Pham, and R. L. Walsworth, Sensitivity optimization for NV-diamond magnetometry, Rev. Mod. Phys. **92**, 015004 (2020).
[55] N. Rach, M. M. Müller, T. Calarco, and S. Montangero, Dressing the chopped-random-basis optimization: A bandwidth-limited access to the trap-free landscape, Phys. Rev. A **92**, 062343 (2015).
[56] M. C. Wang and G. E. Uhlenbeck, On the theory of the Brownian motion II, Rev. Mod. Phys. **17**, 323 (1945).
[57] D. T. Gillespie, The mathematics of Brownian motion and Johnson noise, Am. J. Phys. **64**, 225 (1996).
[58] M. F. Pascual-Winter, R.-C. Tongning, T. Chanelière, and J.-L. Le Gouët, Spin coherence lifetime extension in Tm^{3+}:YAG through dynamical decoupling, Phys. Rev. B **86**, 184301 (2012).
[59] N. Bar-Gill, L. M. Pham, A. Jarmola, D. Budker, and R. L. Walsworth, Solid-state electronic spin coherence time approaching one second, Nat. Commun. **4**, 1 (2013).
[60] G. T. Genov, N. Aharon, F. Jelezko, and A. Retzker, Mixed dynamical decoupling, Quantum Sci. Technol. **4**, 035010 (2019).
[61] G. T. Genov, Y. Ben-Shalom, F. Jelezko, A. Retzker, and N. Bar-Gill, Efficient and robust signal sensing by sequences of adiabatic chirped pulses, Phys. Rev. Res. **2**, 033216 (2020).
[62] N. Aharon, I. Cohen, F. Jelezko, and A. Retzker, Fully robust qubit in atomic and molecular three-level systems, New J. Phys. **18**, 123012 (2016).
[63] J. F. Barry, M. H. Steinecker, S. T. Alsid, J. Majumder, L. M. Pham, M. F. O'Keeffe, and D. A. Braje, Sensitive ac and dc magnetometry with nitrogen-vacancy-center ensembles in diamond, Phys. Rev. Appl. **22**, 044069 (2024).
[64] J. R. Maze, A. Dréau, V. Waselowski, H. Duarte, J.-F. Roch, and V. Jacques, Free induction decay of single spins in diamond, New J. Phys. **14**, 103041 (2012).
[65] D. d'Alessandro, *Introduction to Quantum Control and Dynamics* (Chapman and Hall/CRC, New York, 2021), 10.1201/9781003051268.
[66] M. M. Müller, R. S. Said, F. Jelezko, T. Calarco, and S. Montangero, One decade of quantum optimal control in the chopped random basis, Rep. Prog. Phys. **85**, 076001 (2022).
[67] P. J. Vetter, T. Reisser, M. G. Hirsch, T. Calarco, F. Motzoi, F. Jelezko, and M. M. Müller, Gate-set evaluation metrics for closed-loop optimal control on nitrogen-vacancy center ensembles in diamond, npj Quantum Inf. **10**, 96 (2024).
[68] E. L. Hahn, Spin echoes, Phys. Rev. **80**, 580 (1950).
[69] L. Viola and S. Lloyd, Dynamical suppression of decoherence in two-state quantum systems, Phys. Rev. A **58**, 2733 (1998).
[70] S. Meiboom and D. Gill, Modified spin-echo method for measuring nuclear relaxation times, Rev. Sci. Instrum. **29**, 688 (1958).
[71] T. Gullion, D. B. Baker, and M. S. Conradi, New, compensated carr-purcell sequences, J. Magn. Reson. (1969) **89**, 479 (1990).
[72] G. S. Uhrig, Keeping a quantum bit alive by optimized π-pulse sequences, Phys. Rev. Lett. **98**, 100504 (2007).
[73] C. A. Ryan, J. S. Hodges, and D. G. Cory, Robust decoupling techniques to extend quantum coherence in diamond, Phys. Rev. Lett. **105**, 200402 (2010).
[74] A. M. Souza, G. A. Álvarez, and D. Suter, Robust dynamical decoupling for quantum computing and quantum memory, Phys. Rev. Lett. **106**, 240501 (2011).

[75] A. M. Souza, G. A. Álvarez, and D. Suter, Robust dynamical decoupling, Phil. Trans. R. Soc. A **370**, 4748 (2012).
[76] G. T. Genov, D. Schraft, N. V. Vitanov, and T. Halfmann, Arbitrarily accurate pulse sequences for robust dynamical decoupling, Phys. Rev. Lett. **118**, 133202 (2017).
[77] N. Ezzell, B. Pokharel, L. Tewala, G. Quiroz, and D. A. Lidar, Dynamical decoupling for superconducting qubits: A performance survey, Phys. Rev. Appl. **20**, 064027 (2023).
[78] M. Rossignolo, T. Reisser, A. Marshall, P. Rembold, A. Pagano, P. J. Vetter, R. S. Said, M. M. Müller, F. Motzoi, T. Calarco, F. Jelezko, and S. Montangero, QuOCS: The quantum optimal control suite, Comput. Phys. Commun. **291**, 108782 (2023).
[79] J. Zhang and D. Suter, Experimental protection of two-qubit quantum gates against environmental noise by dynamical decoupling, Phys. Rev. Lett. **115**, 110502 (2015).
[80] H. H. Vallabhapurapu, C. Adambukulam, A. Saraiva, and A. Laucht, Indirect control of the $^{29}SiV^-$ nuclear spin in diamond, Phys. Rev. B **105**, 205435 (2022).
[81] J. Zhang, S. S. Hegde, and D. Suter, Improved indirect control of nuclear spins in diamond N-V centers, Phys. Rev. Appl. **12**, 064047 (2019).
[82] S. S. Hegde, J. Zhang, and D. Suter, Efficient quantum gates for individual nuclear spin qubits by indirect control, Phys. Rev. Lett. **124**, 220501 (2020).
[83] F. Zhang, J. Xing, X. Hu, X. Pan, and G. Long, Coupling-selective quantum optimal control in weak-coupling NV-^{13}C system, AAPPS Bull. **33**, 2 (2023).
[84] F. Dolde, V. Bergholm, Y. Wang, I. Jakobi, B. Naydenov, S. Pezzagna, J. Meijer, F. Jelezko, P. Neumann, T. Schulte-Herbrüggen *et al.*, High-fidelity spin entanglement using optimal control, Nat. Commun. **5**, 3371 (2014).
[85] C. P. Michaels, J. Arjona Martínez, R. Debroux, R. A. Parker, A. M. Stramma, L. I. Huber, C. M. Purser, M. Atatüre, and D. A. Gangloff, Multidimensional cluster states using a single spin-photon interface coupled strongly to an intrinsic nuclear register, Quantum **5**, 565 (2021).
[86] C. E. Bradley, J. Randall, M. H. Abobeih, R. C. Berrevoets, M. J. Degen, M. A. Bakker, M. Markham, D. J. Twitchen, and T. H. Taminiau, A ten-qubit solid-state spin register with quantum memory up to one minute, Phys. Rev. X **9**, 031045 (2019).
[87] G. Van de Stolpe, D. Kwiatkowski, C. Bradley, J. Randall, M. Abobeih, S. Breitweiser, L. Bassett, M. Markham, D. Twitchen, and T. Taminiau, Mapping a 50-spin-qubit network through correlated sensing, Nat. Commun. **15**, 2006 (2024).
[88] M. Zahedian, V. Vorobyov, and J. Wrachtrup, Blueprint for efficient nuclear spin characterization with color centers, Phys. Rev. B **109**, 214111 (2024).
[89] T. Joas, F. Ferlemann, R. Sailer, P. J. Vetter, J. Zhang, R. S. Said, T. Teraji, S. Onoda, T. Calarco, G. Genov *et al.*, High-fidelity electron spin gates in a scalable diamond quantum register, arXiv:2406.04199.